20 CT Angiography of the Thoracic Aorta

G. D. Rubin

CONTENTS

Introduction

Although aortography has long been considered the standard for aortic imaging, there are several reasons why spiral or helical CT may be superior to conventional arteriography for assessing the thoracic aorta. Firstly, the volumetric acquisition of spiral CT enables clear delineation of the aortic arch, tortuous brachiocephalic arterial branches, and adjacent aneurysms and pseudoaneurysms. Because aortography is a projectional technique, the commonly occurring overlap of these structures can confound their visualization and delineation of anatomic relationships. Secondly, blood-pool imaging provided by the intravenous administration of iodinated contrast media allows simultaneous visualization of true and false luminal flow channels, intramural hematomas communicating with the aortic lumen, and slow perigraft flow around thoracic aortic stent grafts. Finally, the aortic wall and non-communicating intramural collections are directly visualized. These advantages together with the rapid, non-invasive means with which CT angiography (CTA) is acquired has resulted in CTA challenging conventional arteriography for the assessment of many thoracic aortic abnormalities. The purpose of this chapter is to review the technical factors that must be considered when acquiring and interpreting thoracic aortic CT angiograms as well as the range of disease states for which CTA can be valuable.

20.1 Imaging Techniques

The first step in performing thoracic aortic CTA is to determine the anatomic coverage required to assess the clinical question. At a minimum, the initiation point of the CT scan should be at the base of the neck so that the proximal aspect of the common carotid and vertebral arteries are included within the CT scan. Inferiorly, coverage should extend to include the origin of the celiac axis. The inclusion of the supra-aortic branches is important when lesions involving the aortic arch extend into these brachiocephalic branches, which commonly occurs in the setting of both aneurysmal disease and aortic dissection. The purpose of including the celiac origin is that lesions of the distal thoracic aorta can be accurately localized relative to this anatomic landmark, which can greatly facilitate planning of endovascular and open repair. There may be some instances when additional anatomic coverage is necessary. For example, in the setting of acute aortic dissection, frequently imaging through the abdomen and pelvis is necessary due to signs and symptoms of diminished blood flow to the abdominal viscera or lower extremity. Similarly, some disease processes may warrant inclusion of portions of the upper extremities particularly when assessing for sources of embolization to the hands.

G. D. Rubin, MD
Department of Radiology, S-072, Stanford University School of Medicine, Stanford, California 94305-5105, USA

Finally, occasionally, a greater degree of anatomic coverage to include the entirety of the carotid arterial circulation may be warranted, particularly in the setting of assessment of large vessel arteritis and aortic dissection associated with symptoms of cerebral ischemia.

To ensure that all relevant anatomy is included in the CT angiograms, thoracic aortic CT angiography begins with a relatively thick section unenhanced localizing scan prescribed from a frontal scout view of the chest and upper abdomen. Usually, 5-mm nominal section thickness associated with a high pitch (2.0 for SDCT and 1.3–1.7 for MDCT) is sufficient to localize the relevant landmarks; however, there are several clinical scenarios where thinner sections should be acquired for these unenhanced views. Specifically, when the assessment is for acute chest pain and intramural hematoma is a diagnostic consideration, unenhanced views can be very valuable for identifying a hyperattenuative mural crescent corresponding to the intramural hematoma. Because 10-mm-thick sections can result in substantial volume averaging, 5-mm nominal thick sections are advised for the unenhanced portion of the scan in this setting. Additionally, when assessing stent grafts, 5-mm-thick unenhanced sections can be useful for mapping the location of calcifications around the stent graft, which can subsequently mimic an endoleak following contrast administration. Because these initial unenhanced scans are thick, a relatively low tube current and potential is satisfactory for this acquisition. We typically use 120 kV and 100 mA. Not only does this dose save radiation exposure to the patient, it also minimizes tube heating that can subsequently limit the current at which the X-ray tube is operated for single-detector-row CT when acquiring the CTA.

Based on these localizing sections, the initiation point and terminus of the CT angiograms, as well as the field of view for reconstruction, is determined.

20.2
Contrast Medium

Prior to performing the CT angiogram, the iodinated contrast administration protocol must be determined. As a general rule, we do not perform CT angiography at a flow rate less than 4 ml/s and for thoracic aortic CT angiograms with durations less than 20 s we prefer at least 5 ml/s injection rate. The duration of the bolus should be equivalent to the duration of the CT scan, and therefore the volume of contrast required is determined by multiplying the CT scan duration by the flow rate. We have found that a volume of at least 80 ml of iodinated contrast medium (350 mg of iodine/ml) is necessary for reliable opacification. This volume of contrast medium at the recommended flow rate is readily delivered through a 20- or 22-G antecubital intravenous catheter. Because highly attenuative undiluted contrast medium within the in-flowing veins can obscure adjacent structures, we always perform thoracic aortic CT angiography through a right antecubital venous source to avoid opacification of the left brachiocephalic vein which can substantially obscure the origins of the brachiocephalic, left, common carotid, and left subclavian arteries. Because of the high flow rates employed in CTA, iodinated contrast medium should always be non-ionic.

The final and critical step for optimizing contrast medium delivery is the determination of the scan delay time following initiation of the contrast medium bolus. In the past we relied upon a preliminary injection of 15 ml of iodinated contrast medium coupled with serial CT sections acquired within the proximal descending aorta to obtain a time-attenuation curve. We selected the time from the initiation of the injection to the peak of this curve as the scan delay for the CT angiogram. The availability of automated scan-triggering capabilities on the CT scanner has led us to abandon this approach. On our CT scanners equipped with this feature, approximately 8 s is required from the time that contrast medium arrives in the descending aorta until the enhancement is recognized and the CTA acquisition is initiated; therefore, we determine the injection duration to be equal to the scan duration plus 8 s. We have found this direct method of visualizing aortic enhancement to be the most reliable method for achieving consistently high-quality CT angiograms.

20.3
CTA Acquisition

Thoracic aortic CT angiography should be performed with a nominal section thickness of 3 mm or less coupled with a relatively high pitch value of 2.0 for SDCT and 1.3–1.7 for MDCT. A 1.25-mm section thickness is not required for the majority of thoracic aortic applications; however, it can be of particular value when a detailed assessment of the supra-aortic branches is indicated. The gantry rotation period should be minimized to the lowest

value available in order to minimize the duration of the acquisition and the dosage of contrast medium. Occasionally, larger patients may benefit from the use of a slower gantry rotation period to overcome excessive image noise, thus enabling a higher mA•S product. Recently introduced techniques for cardiac gating of CT data may prove valuable in the assessment of the ascending aorta and in particular the coronary arteries; however, these techniques are not widespread and therefore are not discussed further in this chapter.

The CT angiogram should be performed within a single breath hold. If breath holding is not possible due to mechanical ventilation of the patient or extreme dyspnea, attempts should be made to avoid sudden gasps for air by allowing the patient to breathe quietly throughout the acquisition rather than attempting a breath hold that cannot be completed.

For the vast majority of CT angiograms, an arterial phase acquisition is sufficient; however, for the assessment of stent-graft repair of aortic aneurysm, delayed views can be very important to assess for endoleak. We typically acquire these views 70 s after the initiation of the arterial phase acquisition and use 2.5- to 5-mm nominal section thickness through the stent graft.

20.4
Reconstruction

The CT angiogram and delayed views when acquired should be reconstructed with an interval that is equivalent to 50% of the effective section thickness. For most acquisitions, a 1.5-mm reconstruction interval is appropriate. The reconstruction field of view should be minimized to only include the relevant arterial anatomy and typically ranges between 25 and 30 cm. We usually use a soft or standard reconstruction algorithm for CT angiograms as these reconstruction algorithms minimize noise in the data which greatly facilitate the creation of 3D views.

A detailed description of 3D rendering is beyond the scope of this chapter. In general, we find the use of curved planar reformations, volume renderings, and shaded-surface displays (SSD) most useful for assessing the thoracic aorta. Furthermore, thin-slab maximum intensity projections (MIP) may be useful; however, full-volume MIPs are rarely useful in the thoracic aorta. A more detailed discussion of these techniques is given below.

20.5
SDCT vs MDCT

For imaging of the thoracic aorta, single-detector-row CT (SDCT) scanners are adequate for the majority of applications; however, MDCT typically results in superior image quality. This is because MDCT scans are usually acquired with narrower effective section thickness, and a shorter period of time, and with less contrast medium. In particular, the shorter scan duration allows for substantially shorter breath-hold periods and more consistent enhancement across the scan acquisition. Furthermore, diminished pulsation-related artifacts through the heart and great vessels have been observed with MDCT (Fig. 20.1). A final consequence of the use of MDCT is that the shorter scan time results in a substantial reduction in contrast medium utilization (Rubin et al. 2000).

Imaging of extended vascular territories beyond the thorax and in particular through the abdomen and pelvis require the use of MDCT to image the entire volume within a single breath hold. The use of SDCT limits the application of thoracic CT aortography to the thoracic aorta alone (Fig. 20.2).

20.6
Technical Considerations for Interpretation

The interpretation of thoracic aortic CT angiograms is greatly facilitated by the use of a workstation to perform soft-copy reading. Scrolling through a stack of transverse sections allows easy integration of the longitudinal dimension in these large three-dimensional data sets. Moreover, substantial variations in the degree of aortic enhancement requires customization of window width and level settings. It is important to adjust the display setting to ensure that the aortic lumen does not appear to be white to facilitate discrimination of luminal enhancement from mural calcifications. Additionally, when assessing delayed images for endoleaks following stent-graft repair, very narrow windows are frequently required for the detection of subtle endoleaks.

20.6.1
Common Artifacts in Thoracic CTA

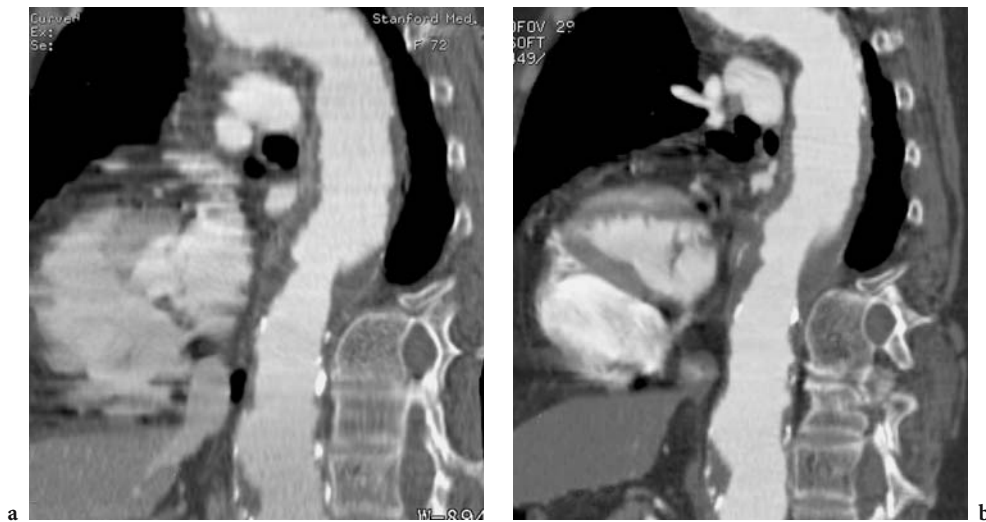Two artifacts result in the majority of interpretative limitations of thoracic aortic CTA: perivenous streaks

Fig. 20.1. a Single-detector CT (SDCT) and **b** multidetector-row CT (MDCT) curved planar reformations through the thoracic aorta in a patient with extensive descending aortic atherosclerotic plaque. These two scans illustrate important differences between SDCT and MDCT acquisitions. The SDCT acquisition (3-mm collimation, pitch 2) demonstrates substantial pulsation-related misregistration artifacts throughout the heart as well as in the left pulmonary artery. These artifacts are reduced on the MDCT scan, particularly in the left pulmonary artery and the left and right ventricles. This is due to the substantially greater table speed of the 2.5 mm, pitch 6.0, acquisition resulting in the heart being imaged in substantially fewer heartbeats
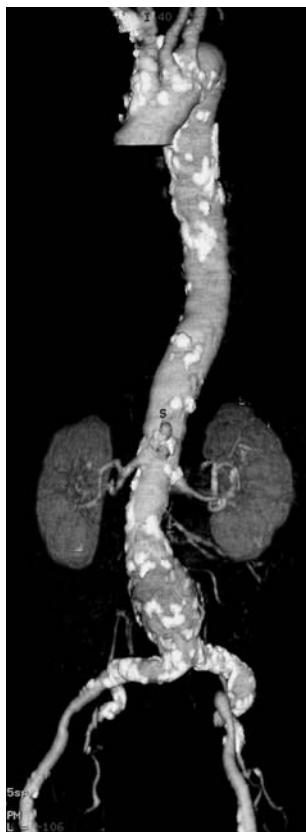

Fig. 20.2. Volume rendering of MDCT angiogram from the thoracic inlet through the common femoral arteries. These emanations required 28 s to image 510 mm with 2.5-mm-thick sections

and arterial pulsation. Both of these artifacts tend to have their greatest influence on the visualization of the ascending aorta and therefore are particularly important to bear in mind when assessing patients suspected of aortic dissection.

Perivenous streaks are likely caused by a combination of beam hardening and motion caused by transmitted pulsation in veins carrying undiluted contrast medium to the heart. Strategies designed to minimize this artifact include the use of dilute contrast medium solutions (REMY-JARDIN et al. 1992; RUBIN et al. 1996b), caudal to cranial scan direction, and femoral venous access (PROKOP et al. 1993). In practice, perivenous streaks are rarely confused with intimal dissection in the ascending aorta as their orientation typically varies from section to section and they typically extend beyond the confines of the aortic wall. The most problematic region for perivenous artifacts is the origin of the supra-aortic branches adjacent to an opacified left brachiocephalic vein. Perivenous streaks in this region can mask extension of intimal flaps into these branches as well as occlusive disease caused by atherosclerotic plaque at their origins. If detected at the time of initial section reconstruction (within 2 min of bolus initiation), then delayed sections can be rapidly prescribed to enable reimaging during a second pass of arterial contrast prior to the equilibrium phase. Other than this rapid intervention and reinjection at another site, there are no techniques to adequately overcome

obscured brachiocephalic arterial origins once the equilibrium phase has begun. The best prevention of this limitation is ensuring that peripheral venous access is from the right upper extremity.

Arterial pulsation has been recognized as a cause of false-positive aortic dissection on conventional and helical CT scans. The increasing acquisition speed of helical CT scanners may ultimately result in the elimination of this artifact; however, in the meantime there is an intervention that can be retrospectively applied to the raw scan data to minimize these artifacts. "Segmented" or "weighted half-scan" reconstruction is an alternative interpolation technique that minimizes the amount of projection data required to generate a cross section. As implemented by General Electric, this results in a reduction of projection data required to reconstruct a cross section from the standard 360 to 225°. For a 1-s gantry rotation period, segmented reconstruction effectively increases the temporal resolution of the CT scan from 1 to 0.6 s. This has been demonstrated to eliminate artifacts that might be misconstrued as intimal flaps on conventional CT scans (Posniak et al. 1993). It is available for helical scans as well. Its use is typically required if an equivocal finding is present on a single image and should not be considered necessary when linear filling defects are visualized entirely within the confines of the aortic wall on sequential reconstructions – an indication of a true intimal flap (Fig. 20.3).

Arterial pulsation and perivenous streaks can also create distractions on SSDs and MIPs, even after the superior vena cava has been edited from the data. Aortic pulsation, which tends to be more pronounced in thinner individuals, results in a serrated appearance to arteries, which can mimic fibromuscular dysplasia in blood vessels such as renal arteries, but is rarely a limitation in the chest. It is useful to always bear in mind the discordance between gantry rotation and cardiac pulsation, which can explain some unusual CT images.

Because the cardiac period is spread over a longer distance longitudinally as the table speed of the CT scanner increases, pulsation artifacts are less frequent with the higher table speeds found with MDCT (Rubin et al. 2000). As gantry rotation period diminishes from 2 to 1 to 0.8 to 0.5 s, the temporal resolution of the scan improves and variations in aortic position appear more discrete, thus accentuating pulsation artifacts. Longer gantry rotation will smooth these artifacts due to smearing of the information over a longer period of time. An extreme example of this condition occurs during gadolinium-enhanced 3D MRA, where data are acquired for each anatomic location across the entire acquisition. The result is a very smooth appearing aortic surface, the

Fig. 20.3. *Top row:* Contiguous 3.75-mm transverse section MDCT sections obtained through the ascending aorta in a patient who had been run over by a tractor. Acquisition parameters are 3.75-mm detector width, pitch 6.0, table speed of 22.5 mm per rotation, and 0.8 s per rotation. An apparent linear filling defect is present within the ascending aorta on all three sections. This filling defect persisted even with the reconstruction of overlapping sections (not shown). *Bottom row:* Identical image locations from the same CT acquisition reconstructed with a half scan or segmented reconstruction algorithm. The segmented reconstruction requires approximately 220° of data resulting in an effective temporal resolution of 0.5 mm. By reconstructing the sections using this algorithm, the apparent linear filling defects are revealed to be motion-related artifacts, and thus there is no suspicion for ascending aortic injury
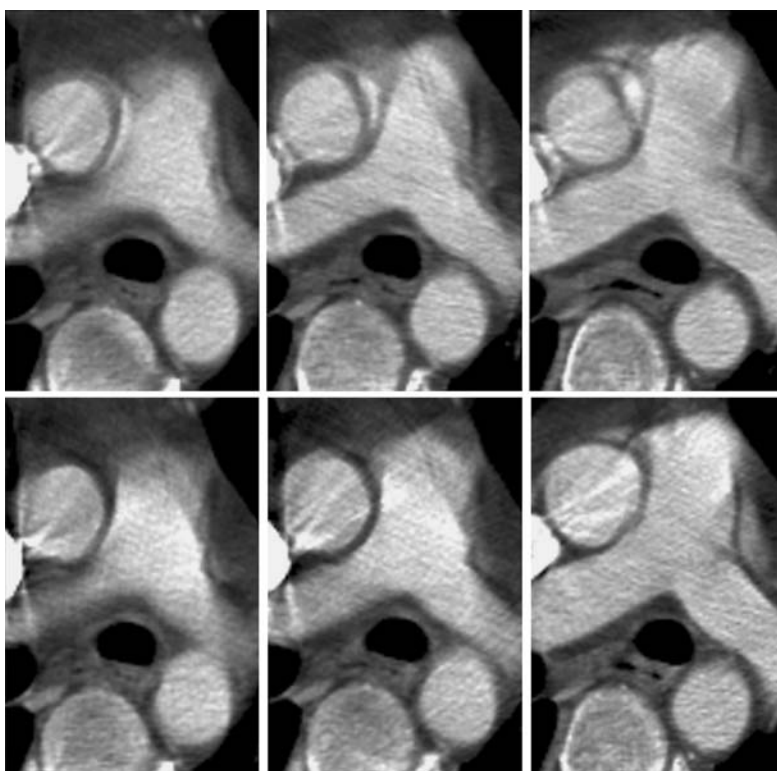
position of which represents the average position of the aorta across the entire acquisition.

20.7
Alternative Visualization: Reformation and Rendering

Although primary reconstructed transverse sections remain the mainstay of CTA interpretation, alternative visualization techniques can substantially augment diagnosis and provide an efficient means of communicating critical anatomic relationships to referring clinicians. The four most popular means of alternative visualization for CTA data: multiplanar reformation (MPR); SSD; MIP; and volume rendering (VR).

The MPR, which includes curved planar reformations (CPR) as well as traditional sagittal, coronal, and oblique tomograms, are typically a single voxel thick, but all MPRs can be broadened by combining information from adjacent voxels to obtain a thickened tomogram, referred to as a thin-slab or multi-planar volume rendered (MPVR) view (NAPEL et al. 1993). The thickness of the slab and method with which the slab is computed are user specified. The advantage of displaying anatomy with thin slabs is that pre-rendering segmentation or editing is not required, and some of the difficulties inherent in demonstrating vessel origins that originate in different but nearby planes, such as occurs with the branches of the aortic arch, are overcome. Despite these advantages, however, the single-voxel thick tomogram, particularly the CPR, is the most useful of the MPR techniques (RUBIN et al. 1995). Its advantage is best appreciated when visualization of the luminal contents of the aorta or its branches is critical, such as in cases of aortic dissection or aortic stent-graft deployment. The relationship of intimal flaps to branch ostia can be well depicted, mural thrombus, atheroma, or hematoma to the flow lumen and branch ostia, and the interior of stents or stent grafts can be assessed for stenosis from neointima or for branch origin stenosis due to overlying graft material.

As commonly implemented, SSDs (CLINE et al. 1991; MAGNUSSON et al. 1991) are relatively simple three-dimensional views that render the entire volume or an edited subvolume to display complex three-dimensional relationships, particularly in regions of vessel overlap. The typical implementation on imaging workstations begins with the application of a single threshold value which converts the 12-bit deep CT data into a binary or 1-bit data set – above

or below the threshold value. While this approach may result in artifacts and misrepresentation of the anatomy, the arbitrary selection of a threshold value or the necessity to select only a single threshold value is most limiting clinically when assessing vascular occlusive disease for stenosis grading, differentiating calcified plaque from luminal enhancement, and visualizing mural thrombus (RUBIN et al. 1994, 1995). For the most part, thoracic aortic disease is not occlusive, but rather aneurysmal (true or false), aberrant branching (congenital), and intimal dissection or intramural hematoma. For all of these applications with the exception of intramural hematomas and some thrombosed false lumina, SSD provides the best simulation of lesion anatomy for surgical planning.

Maximum intensity projections (RUBIN et al. 1994; KELLER et al. 1989; NAPEL et al. 1992), while of value for CTA of other vascular territories, has limited applicability when assessing the thoracic aorta outside of thick-slab or MPVR applications. Calcified atheroma by itself is rarely of clinical significance, and the configuration of the aortic arch and its adjacency to other opacified structures, such as pulmonary arteries and veins, results in substantial vessel overlap; therefore, when assessing the thoracic aorta, the advantage that MIP–CTA allows simultaneous visualization and differentiation of the opacified flow lumen and mural calcium does not offer substantial clinical utility, and the inability of MIP to allow overlapping structures to be discerned is a substantial limitation (Fig. 20.3).

The final and most complex rendering technique is VR (DREBIN et al. 1988; LEVOY 1991; RUSINEK et al. 1989; FISHMAN et al. 1987; RUBIN et al. 1996a). There are many different versions and interfaces for VR, but the general approach is that all voxel values are assigned an opacity level that varies from total transparency to total opacity. This opacity function can be applied to the histogram of voxel values as a whole or to regions of the histogram that are classified as specific tissue types. With the latter approach, rectangular or trapezoidal regions are selected that correspond to the range of attenuation values for a structure (JOHNSON et al. 1996; KUSZYK et al. 1996). The "walls" of the trapezoid slope from an opacity plateau to the baseline of complete transparency in an attempt to account for partial-volume effects at the edges of structures. Regions at the walls of the trapezoidal regions or in positions where the opacity curve has a steep slope are referred to as transition zones in the ensuing protocols and are analogous to threshold levels with SSDs. Lighting effects may be simulated in a similar fashion as with SSD. Because

there is no surface definition with VR, lighting effects are applied based on the spatial gradient (i.e., variability of attenuation within a local neighborhood of voxels). Near the edges of structures, the spatial variation in attenuation changes more rapidly (a high gradient) than in the center of structures (a low gradient). Lighting effects are most pronounced in regions of high spatial gradients. Because lighting effects and variations in transparency are simultaneously displayed, it is frequently useful to view VRs in color. The color is applied to the attenuation histogram to allow differentiation of pixel values and to avoid ambiguity with lighting effects, which are encoded in gray scale. Other variables, such as specular reflectivity, which models the "shininess" of a surface, may be available but should be used with caution to avoid confounding the visualization.

20.8
Clinical Applications

20.8.1
Thoracic Aortic Aneurysm

The CTA is a useful tool for diagnosing thoracic aortic aneurysms, determining their extent, and predicting appropriate management (Quint et al. 1996). While the diagnosis of aortic aneurysms is readily made from transverse sections, an assessment of the extent of the lesion, particularly when the brachiocephalic branches are involved, is facilitated by an assessment of CPRs and SSDs (Fig. 20.4).

In general, thoracic aortic aneurysms greater than 5 cm are at an increased risk for rupture. Although thoracic aortic aneurysm expand at a slower rate than abdominal aortic aneurysms, surgical repair is contemplated when thoracic aneurysms reach a diameter of 5–6 cm (Masuda et al. 1992; Dapunt et al. 1994). Helical CT can facilitate surgical planning by delineating the extent of the aneurysm and the involvement of aortic branches. In fact, Quint and colleagues (1996) found that an analysis of transverse sections and multiplanar reformations was 94% accurate with a positive predicative value of 95% and negative predictive value of 93% for successfully predicting the need for hypothermic circulatory arrest. With the exception of the elimination of one false-negative result, the addition of MPRs did not alter the predictions made from the transverse sections alone. Three-dimensional renderings were not evaluated in this study (Quint et al. 1996).

Because of the tortuosity and curvature of the thoracic aorta, aneurysm sizing is performed most accurately when double-oblique tomograms are generated perpendicular to the aortic flow lumen. The challenge of such an approach is that data concerning the risk of aneurysm rupture and expansion rate are based on measurements made from transverse sections, where true diameters can be overestimated. Furthermore, the measurement technique must be reproducible to assess the rate of aneurysm expansion on sequential studies.

The most complete measure of aneurysm size, however, is not the determination of true aortic diameters or even cross-sectional area, but aneurysm volume. Currently, this approach has substantial drawbacks. While the volumetric data of helical CT should be excellent for determining aneurysm volume, the accurate segmentation of both patent, thrombosed, and atheromatous elements of the aorta must be segmented from the adjacent structures to make this determination. The only technique available to perform this is painstaking manual segmentation performed by drawing regions of interest around the aorta on each cross section. Furthermore, to date aneurysm expansion has been studied primarily in terms of radial expansion of the aorta. While aneurysm volume determination is an attractive measure of aneurysm growth based on theoretical considerations, data concerning the risk of aneurysm rupture and guidelines for intervention are based on traditional transverse diameter measurements (Masuda et al. 1992; Dapunt et al. 1994).

20.8.2
Thoracic Aortic Dissection

The critical clinical issue required of any imaging test applied to a patient suspected of having an aortic dissection is the identification of an intimal flap and its localization to the ascending (type A) or descending (type B) aorta. This fundamental diagnostic feature that determines the need for emergent repair can be addressed by at least four imaging modalities: angiography; CT; magnetic resonance imaging (MR); and transesophageal echocardiography (TEE).

The relative accuracy of these modalities has been debated in the medical literature and is confounded by the fact that technical improvements in CT, MR, and TEE have outpaced our ability to compare them in appropriately designed prospective trials. Recent opinion has shifted toward MRI or TEE as the most sensitive tests for aortic dissection (Cigarroa et al. 1993).
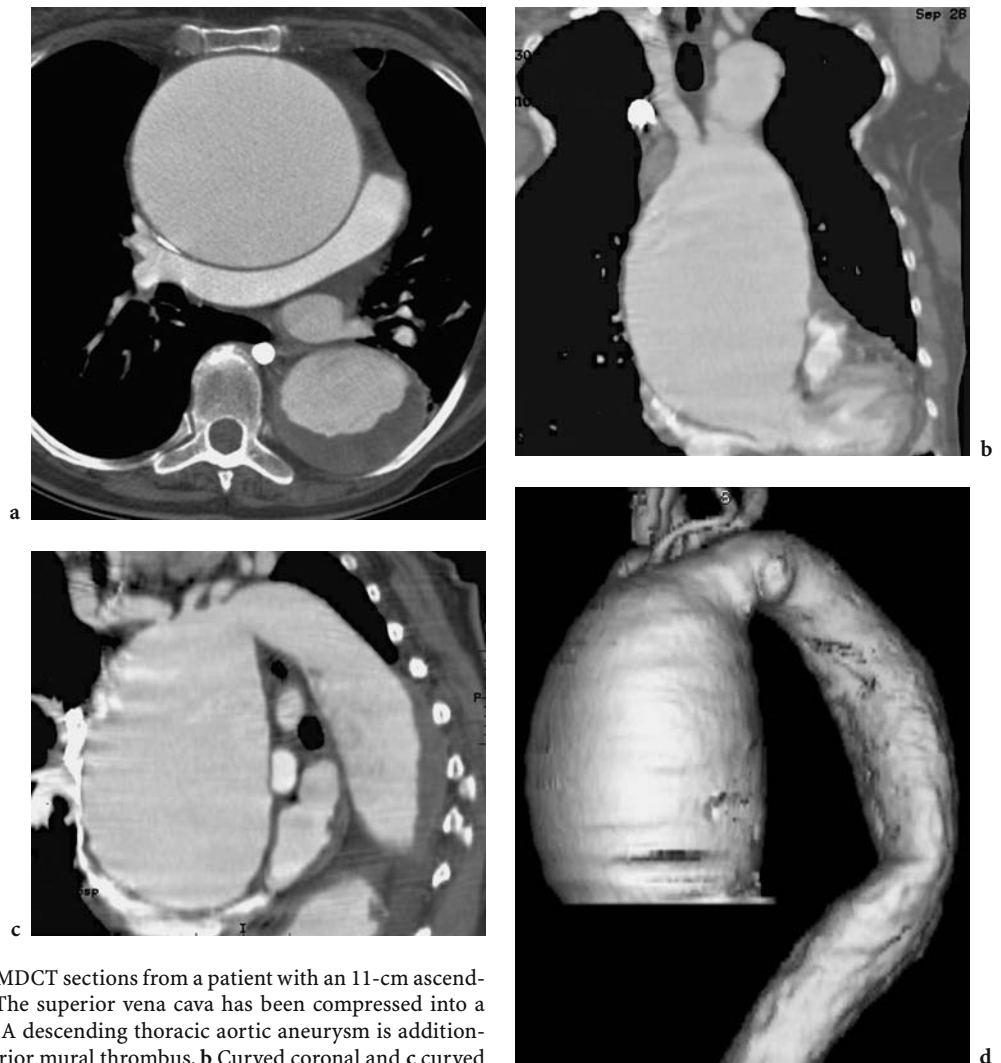
Fig. 20.4. a Transverse MDCT sections from a patient with an 11-cm ascending aortic aneurysm. The superior vena cava has been compressed into a slit-like configuration. A descending thoracic aortic aneurysm is additionally present with posterior mural thrombus. **b** Curved coronal and **c** curved sagittal reformations demonstrate origins of all supra-aortic branches from the ascending aortic aneurysm. The curved coronal reformation (**b**) demonstrates the marked displacement of the left ventricle resulting from this large aneurysm. **d** Shaded-surface display further improves depiction of the full extent of the aneurysm particularly at its distal neck

Unfortunately, much of this opinion is based on comparative studies where state-of-the-art MR or TEE is compared with relatively primitive conventional CT technique (ERBEL et al. 1989; NIENABER et al. 1993). In 1989, ERBEL and colleagues studied 164 consecutive patients with suspected aortic dissection. All patients were studied with transthoracic echocardiography and TEE, 85 patients were studied with CT, and 96 patients were studied with aortography. The technique for CT scanning was 10-mm-thick sections acquired at 20- to 40-mm intervals through the chest. Details of how iodinated contrast was administered are not given. Not surprisingly, CT was found to be less sensitive (77%) than echocardiography (98%)

and aortography (89%) in those patients with surgical proof (ERBEL et al. 1989). In 1993 NIENABER and co-workers compared 110 patients with suspected aortic dissection who underwent at least two of three imaging tests: TEE; CT; or MR. The CT was found to have lower sensitivity (93.8%) than TEE (97.7%) and MR (98.3%) and lower specificity (87.1%) than MR (97.8%). For this study, 80–100 ml of contrast were administered during the course of 5- to 15-min scans that were performed with section intervals of 20 mm (NIENABER et al. 1993). To date, there have been no comparisons of helical CT to either MR or TEE, and while it is tempting to discount these prior studies because of the substantial advances that have

occurred in CT imaging, TEE and MR have undergone further improvements as well.

The TEE has progressively improved with the introduction of biplane and multiplane probes that substantially reduce the blind spots and ambiguous reverberation artifacts that can limit the accuracy of monoplane devices (CIGARROA et al. 1993). Newer MR techniques, employing a dynamic intravenous injection of gadolinium coupled with a rapid breath-held gradient-echo acquisition, have also yielded impressive images that should improve the diagnostic accuracy of MR over that of spin-echo and cine techniques (PRINCE et al. 1996; KRINSKY et al. 1997). The one modality that has not been substantially improved has been conventional angiography. Currently, the primary indication for diagnostic arteriography of acute aortic dissection is in the setting of arrhythmia or ECG abnormalities suggestive of coronary artery involvement and myocardial ischemia. It is likely that in appropriately skilled hands, the accuracy of TEE, CT, and MR will be nearly identical for the diagnosis of aortic dissection. Access to these three modalities is another issue, however.

Because patients suffering from acute aortic dissection are typically critically ill and potentially in need of an emergent operation, expediency of diagnosis is important. In a center where experienced cardiologists are available to perform state-of-the-art TEE in the emergency room to identify the presence of an intimal flap in the ascending aorta, this will likely be the preferred first-line imaging test. An additional advantage of TEE over CT acutely is its ability to identify aortic valvular insufficiency, which in the setting of acute aortic dissection will indicate the need for emergent valve replacement in addition to aortic repair. When high-quality TEE is unavailable, however, in most institutions CT will be the modality that is most accessible and staffed to handle potentially hemodynamically unstable patients (Fig. 20.5).

When considering the clinical utility of a diagnostic test, it is useful to consider the likelihood that a test will suggest an alternative diagnosis when the primary diagnosis is not present. Figure 20.6 illustrates a case where the combination of acute chest pain and diminished right brachial and radial pulses were highly suggestive of aortic dissection. No dissection was identified; however, a high-grade stenosis of the brachiocephalic artery origin and an occluded bypass graft originating on the anterior surface of the ascending aorta and inserting onto a proximally stenosed left anterior descending coronary artery was found on CTA. It is unlikely that either of these abnormalities would have been detected with TEE.

In the setting of chronic aortic dissection or acute dissection that does not necessitate emergent operation, other imaging issues emerge that cannot be addressed by TEE. These include the extension of the intimal flap into aortic branches, true luminal compression by the false lumen limiting blood flow into the abdomen, and the presence of fenestrations that allow communication between the true and false lumen. Clinically relevant aortic branch involvement typically is intraabdominal where mesenteric ischemia, renal insufficiency, and lower extremity claudication indicate extension into mesenteric, renal, and iliac arteries, respectively. Intervention, either surgically or using catheter-based techniques, may be required. The CT appears to be excellent for establishing extension of intimal flaps into aortic branches; however, its accuracy has not been established. When considering catheter-based interventions, preprocedural CT can be very useful. The simultaneous visualization of all aortic lumina can help to avoid confusion in the angiography suite that results from opacification of only one of three or more lumina in a complex dissection. The CT scan can also help identify the best route for achieving access to aortic branches.

While the superior spatial resolution and improved aortic enhancement provided by helical CT results in substantially better images than conventional CT, some pitfalls persist. Pulsation in the ascending aorta can mimic an intimal flap. This artifact tends to be less of a problem with helical CT as the generation of closely overlapping sections in the region of the suspected artifact or intimal flap, displayed sequentially as a cine loop, usually establishes the artifact as rotating or moving relative to the aorta. Examination of wide windows may document extension of artifacts beyond the aortic wall. The use of segmented reconstruction of the helical scan data may eliminate motion artifacts observed on standard reconstructions (POSNIAK et al. 1993). Finally, differential flow in the true and false lumina can result in the spurious appearance of a thrombosed false lumen when scan delay is based upon a timing study directed to the true lumen of the aorta. In the setting of suspected aortic dissection, bolus timing should be performed just below the aortic arch, where transverse cross sections of the distal ascending and proximal descending aorta can be evaluated. A region of interest is placed in both the true and false lumens of and two curves are generated. A delay time that assures some false luminal opacification is selected and the bolus duration then extended by the number of seconds between the true luminal peak and the selected delay
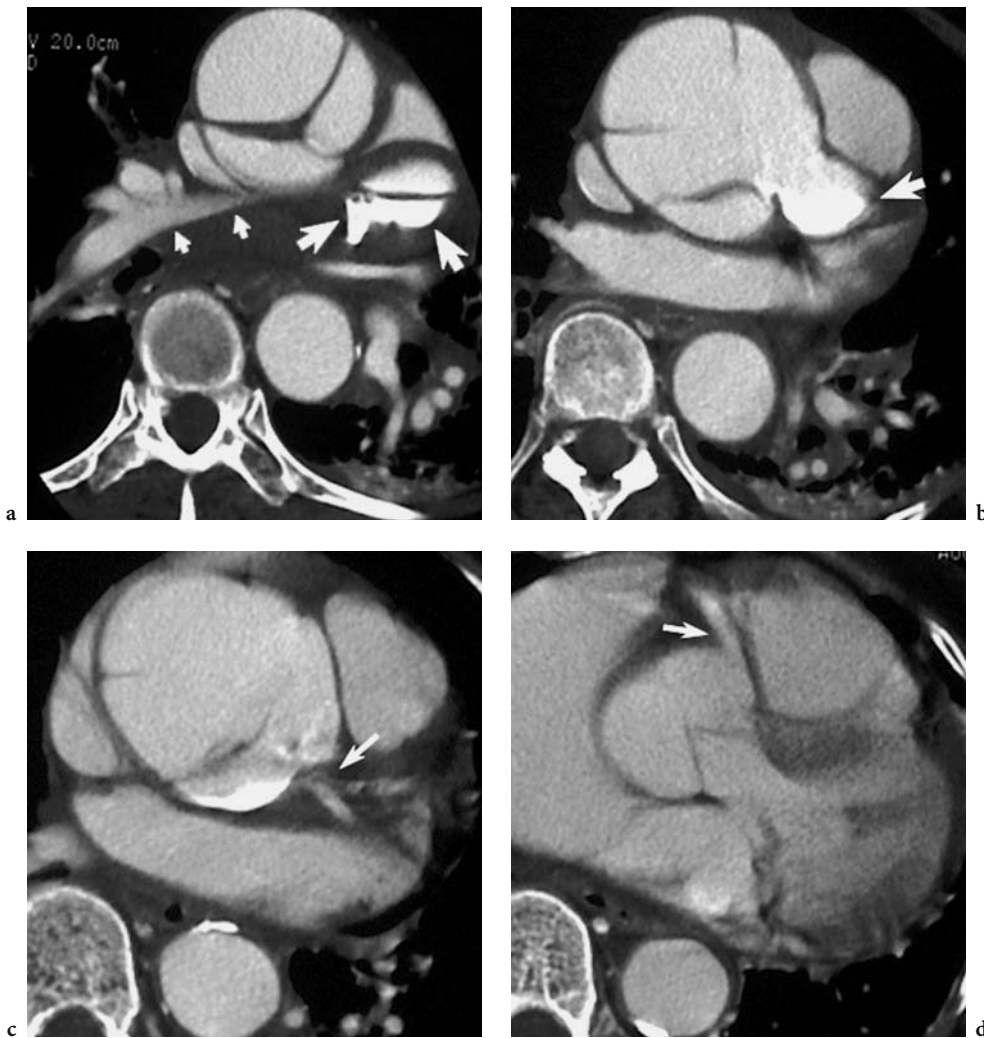
Fig. 20.5. a, b Transverse CT sections in a patient with acute chest pain demonstrates a type-A aortic dissection with posteromedial rupture of the proximal ascending aorta and active extravasation of arterial contrast medium into the mediastinum through a pseudoaneurysm (*large arrows*). A mediastinal hematoma is resulting in substantial right pulmonary arterial compression (*small arrows*). **c** The original left main coronary artery could be visualized one section below this image, which demonstrates the proximal left, centered, and circumflex coronary arteries (*arrow*) originated immediately below the pseudoaneurysm from the left sinus of Valsalva. **d** The right coronary artery origin is clearly uninvolved (*arrow*), as is the aortic valve

time. This assures true and false luminal opacification for the duration of the helical acquisition.

When considering alternative visualization techniques in the setting of aortic dissection, it should not be surprising that MIPs are limited as they do not demonstrate the intimal flap unless it is oriented perpendicular to the MIP. Curved planar reconstructions can be very useful for displaying the flap within the center of the vessel, whereas SSDs depict the interface of the intimal flap with the aortic wall.

20.8.3
Intramural Hematoma

Although initially recognized pathologically in 1920, intramural hematoma has only recently been recognized as a distinct clinical entity from aortic dissection. Several mechanisms have been proposed, including spontaneous rupture of vasa vasorum, intimal fracture at an atherosclerotic plaque, and intramural propagation of hemorrhage adjacent to a penetrating
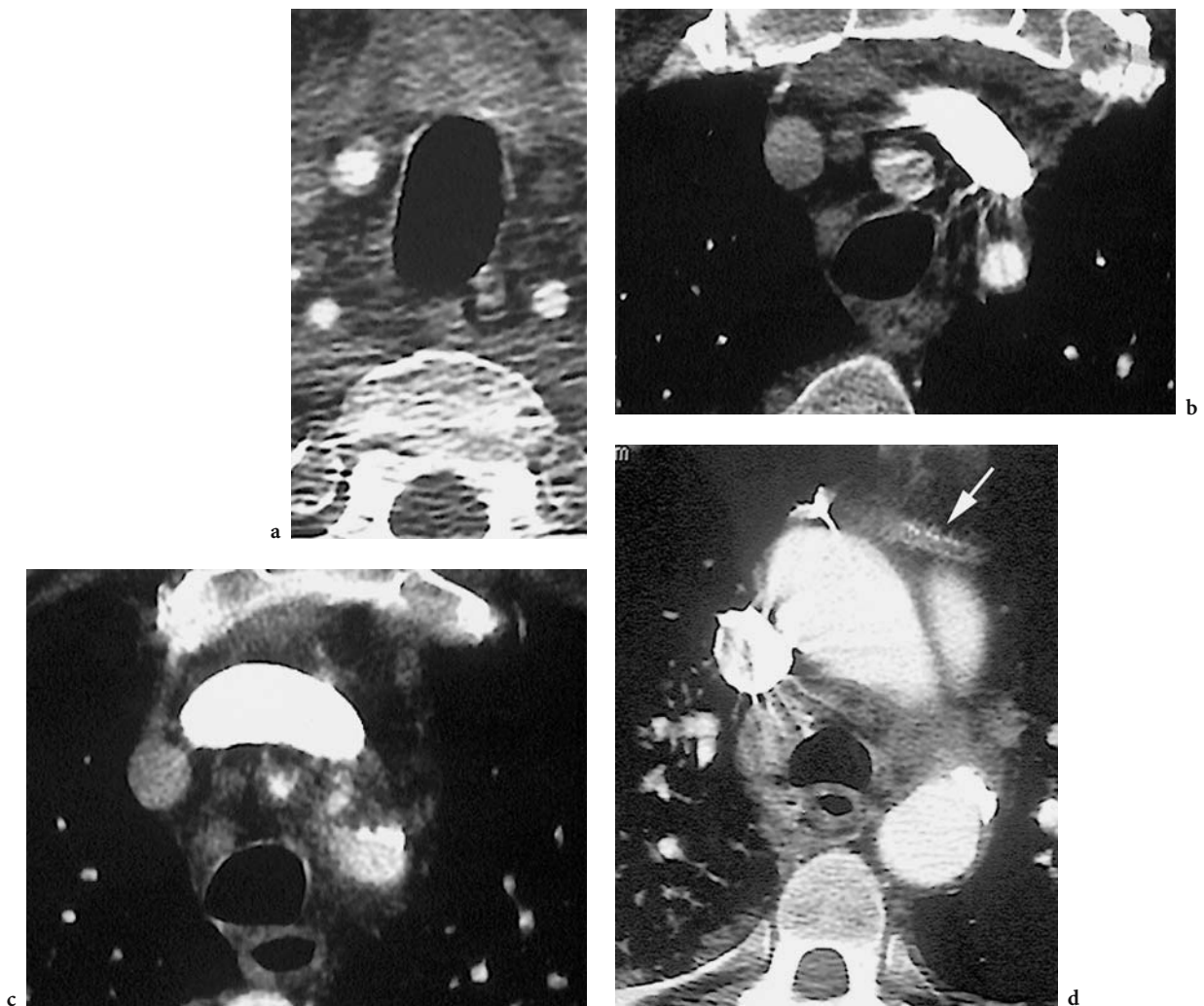
Fig. 20.6. **a–c** Transverse sections acquired with 3-mm collimation and 2.0 pitch in a patient with acute chest pain and diminished right brachial and radial pulses. One centimeter above the aortic arch (**c**), there is a high-grade stenosis of the brachiocephalic artery origin and a narrow left common carotid artery origin. One centimeter cephalad (**b**) the brachiocephalic artery is normal caliber but the left common carotid artery is nearly occluded. At the thoracic inlet (**a**) the left common carotid artery is completely occluded. Note that both vertebral arteries are large in this patient with unsuspected, although substantial, flow limitation into both carotid arteries. Below the aortic arch (**c, d**) a thrombosed coronary artery bypass graft (*arrow*) from the ascending aorta to the left anterior descending coronary artery is demonstrated. The findings were confirmed arteriographically and serial enzymes established the diagnosis of acute myocardial infarction

atherosclerotic ulcer. Regardless of the cause, patients with intramural hematomas exhibit signs and symptoms as well as risk profiles that are virtually identical to classic aortic dissection (NIENABER et al. 1995).

KAZEROONI and co-workers, based on an analysis of conventional CTs in 16 patients, described the CT appearance of intramural hematomas caused by penetrating atherosclerotic ulcers. In addition to the visualization of at least one ulcer in 15 of 16, the intramural hematoma was visualized in all 16, and its subintimal location was confirmed by the observation of displaced intimal calcifications in 13 patients (Fig. 20.7; KAZEROONI et al. 1992). While intramural hematomas associated with ulceration tend to predominate in the descending aorta (KAZEROONI et al. 1992), the distribution of all intramural hematomas was 48% ascending aortic, 8% aortic arch, and 44% descending aortic in one series (NIENABER et al. 1995).

In Quint's series two patients in whom intramural hematomas were identified, but an associated

Fig. 20.7a–d. Transverse CTA sections demonstrate a descending thoracic aortic intramural hematoma associated with marked aortic wall enhancement and thickening (*white arrow*). The subintimal location of the hematoma is confirmed by the presence of intimal calcium on its internal surface (*black arrow*). Ulceration was not identified

ulceration could not be identified, were scored as false-negative examinations (QUINT et al. 1996). Recognizing that intramural hematoma formation has two proposed mechanisms: (a) extension of a penetrating ulcer into the media with subsequent bleeding into the aortic wall; and (b) primary disruption of vasa vasorum without penetrating ulcer formation (KAZEROONI et al. 1992; GORE 1952). The diagnoses in these cases may have been correct given a primary intramural bleed as the mechanism for intramural hematoma formation, which need not be associated with ulceration.

Unenhanced sections typically reveal a high-attenuation crescent within the wall of the aorta (Fig. 20.8). Another finding that is seen in the setting of intramu-

ral hematoma is intense enhancement and thickening of the aortic wall external to the hematoma, which may represent adventitial inflammation.

20.8.4
Thoracic Aortic Trauma

Prior to the introduction of helical CT, unenhanced conventional CT scanning was used to detect mediastinal hemorrhage as an indirect sign of aortic injury. In a meta-analysis of 18 previously published series of post-traumatic thoracic CT revealed that mediastinal hemorrhage had a specificity of 87.1% and a sensitivity of 99.3% for predicting aortic
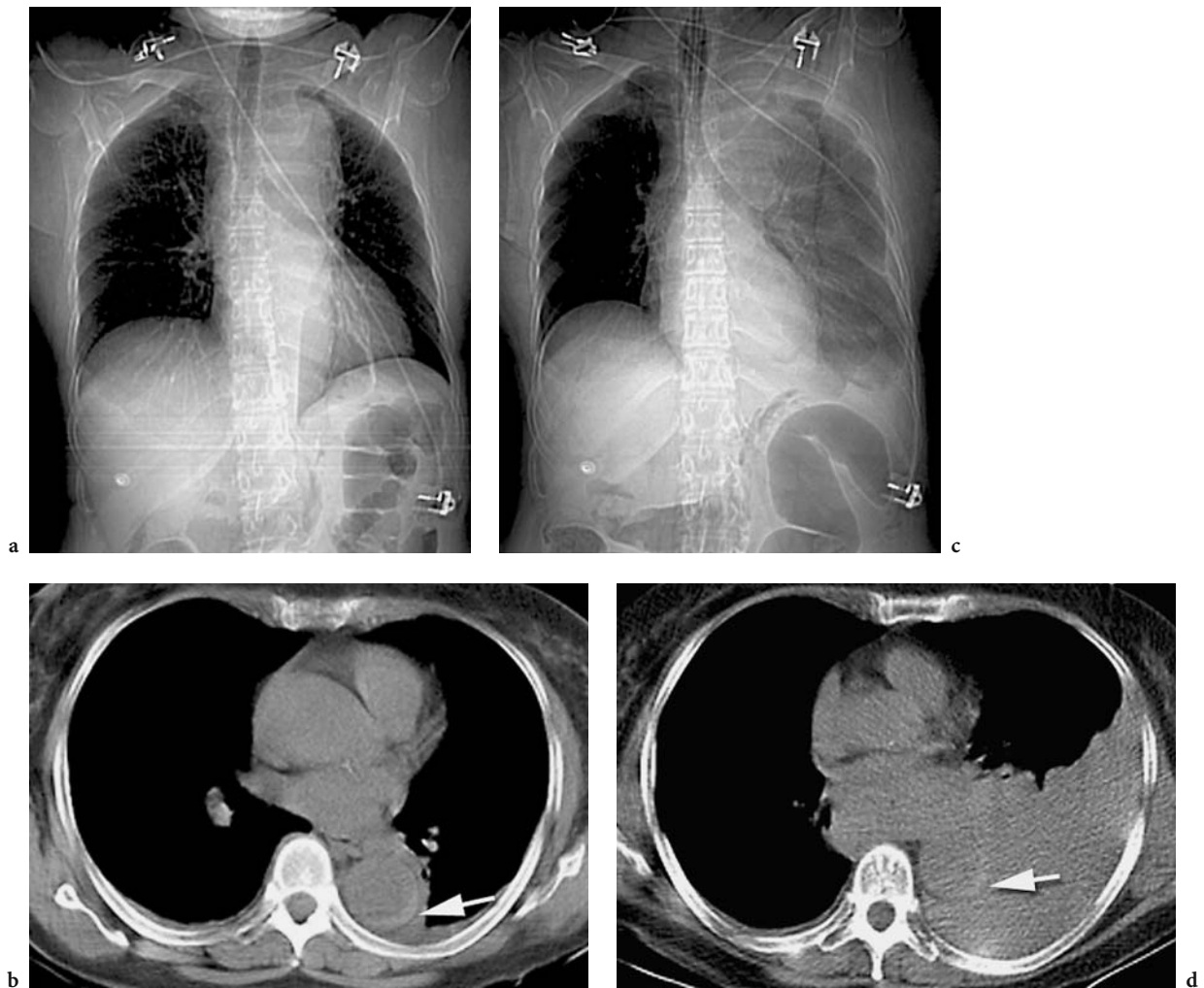
Fig. 20.8. a Frontal projectional radiograph of the chest demonstrates a widened aortic arch in a patient with acute chest pain. **b** Unenhanced transverse CT section obtained in anticipation of performing a CT angiogram demonstrates a high-attenuation crescent within the posterior wall of the descending aorta (*arrow*). A small left pleural effusion is present. This high-attenuation crescent is pathognomonic for an intramural hematoma. Prior to performing the ensuing CT angiogram, the patient became acutely hemodynamically unstable on the CT table necessitating cardiopulmonary resuscitation. **c** Forty-five minutes after the initial acquisition, **a, b** the patient was stabilized hemodynamically. A repeat frontal projectional radiograph demonstrates that the left hemothorax is now filled with fluid. **d** Transverse CT section at this time demonstrates a large left pleural effusion (*arrow*), which was subsequently demonstrated to represent blood due to acute rupture of the aorta at the site of the intramural hematoma. The high-attenuation crescent within the aortic wall, which is now displaced anteriorly, compared with the earlier cross section, is still visible

injury (MIRVIS et al. 1996). Reliance on CT for triaging patients to angiography only when CT was suspicious resulted in an overall cost savings of over $365,000.00 in their own series of 677 trauma patients with chest radiographic abnormalities warranting aortic imaging (MIRVIS et al. 1996). While these results are impressive, many have argued that the confident identification of mediastinal hematoma, particularly on unenhanced CT, is extremely difficult (RAPTOPOULOS 1994), and that the presence of mediastinum hematoma is insufficiently sensitive and specific for thoracic aortic injury.

The application of helical CTA to suspected aortic trauma offers the critical advantage of direct visualization of the aortic tear (Fig. 20.9). Although initial reports did not rely on the use of high-resolution helical acquisitions coupled with high-flow iodinated contrast injections, the results were encouraging. GAVANT and colleagues published the first helical CTA series of aortic injury. Using 7-mm collimation
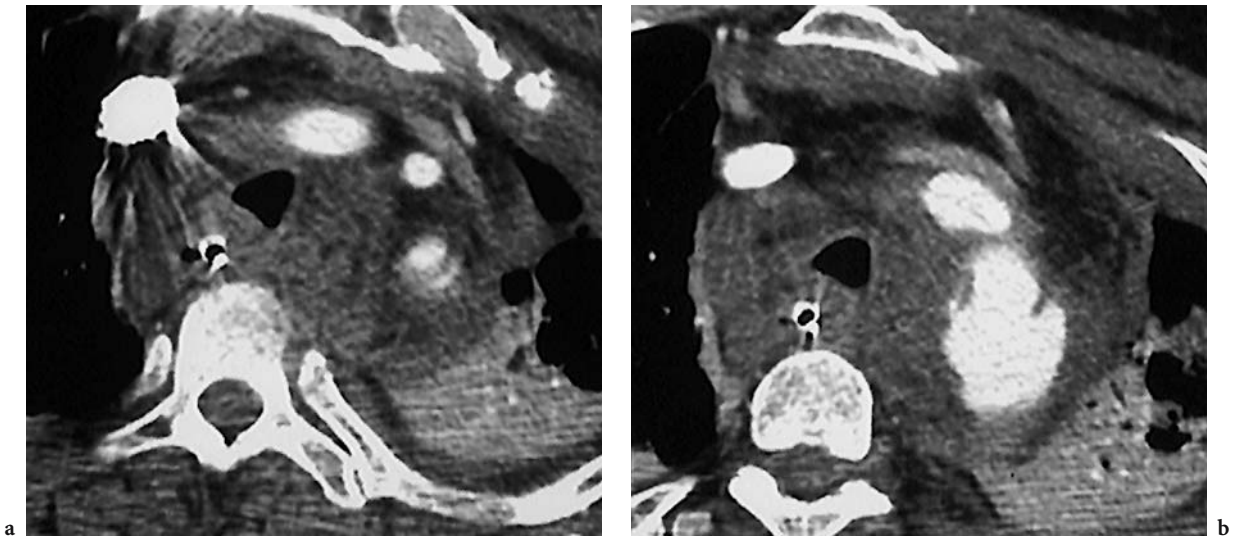
Fig. 20.9a, b. Status after high-speed motor vehicle accident: gross aortic injury. Transverse helical CTA sections demonstrate aortic injury with pseudoaneurysm formation at the aortic isthmus. An intimal injury extends into the left subclavian artery. There is extensive mediastinal hematoma. The findings were confirmed in the operating room

and a contrast medium flow rate of 1.5–2.0 ml/s, they found that the sensitivity of CT was greater than that of conventional arteriography (100 vs 94.4%), but the specificity and positive predictive values were less than those of conventional arteriography (81.7 and 47.4%, respectively, for CT vs 96.3 and 81% for aortography) in a subset of 127 of 1518 patients with nontrivial blunt thoracic trauma who under went both CT and aortography. Perhaps the most encouraging result of this study was that no false-negative results occurred in the 21 patients with aortic injury (GAVANT et al. 1995).

GAVANT subsequently described the CT appearance of 38 thoracic aortic or great vessel injuries in 36 patients identified with helical CT and confirmed with aortography or surgery. Six (17%) of these cases were found to have either no or "difficult-to-detect" para-aortic or mediastinal hematoma. Transverse sections showed either an intimal flap or thrombus protruding into the aortic lumen in all cases. Of 28 injuries to the descending aorta, 23 (82%) were associated with a pseudoaneurysm. In subjectively comparing the value of the reconstructed transverse sections to multiplanar reformations and 3D renderings, the authors felt that the transverse sections were best for depicting the proximal and distal extent of the lesion, and aside from the fact that multiplanar reformations and 3D renderings "portray the thoracic aortic lumen in a familiar light" did not contribute substantially to the identification and characterization of aortic injury (GAVANT et al. 1996).

A recent publication by PARKER and colleagues (2001) reported on an investigation of 142 patients with abnormal chest radiographs following trauma that were suggestive of aortic injury. All patients had CTA and conventional thoracic aortography. The sensitivity and negative predictive value of CT were 100%. Fourteen false-positive CT results occurred and were attributed to a conservative approach where ductus bumps, bronchial artery infundibula, and hemomediastinum (PARKER et al. 2001). Similar results have been reported by DYER and colleagues (1999).

20.8.5
Congenital Anomalies

Congenital anomalies of the thoracic aorta and aberrant branches of the descending aorta such as CT, vascular rings, aberrant supra-aortic branching, coarctation (Fig. 20.10), and enlarged bronchial arteries or major arteriopulmonary communicating arteries are easily diagnosed and characterized (KATZ et al.1995; HOPKINS et al. 1996) with helical CT. The use of conventional angiography for the diagnosis and characterization of lesions such as pulmonary sequestration should no longer be necessary if a thin-section volumetric acquisition is appropriately acquired with adequate contrast enhancement. The simultaneous visualization of the airways complements vascular visualization by allowing a direct determination of the specific structures responsible
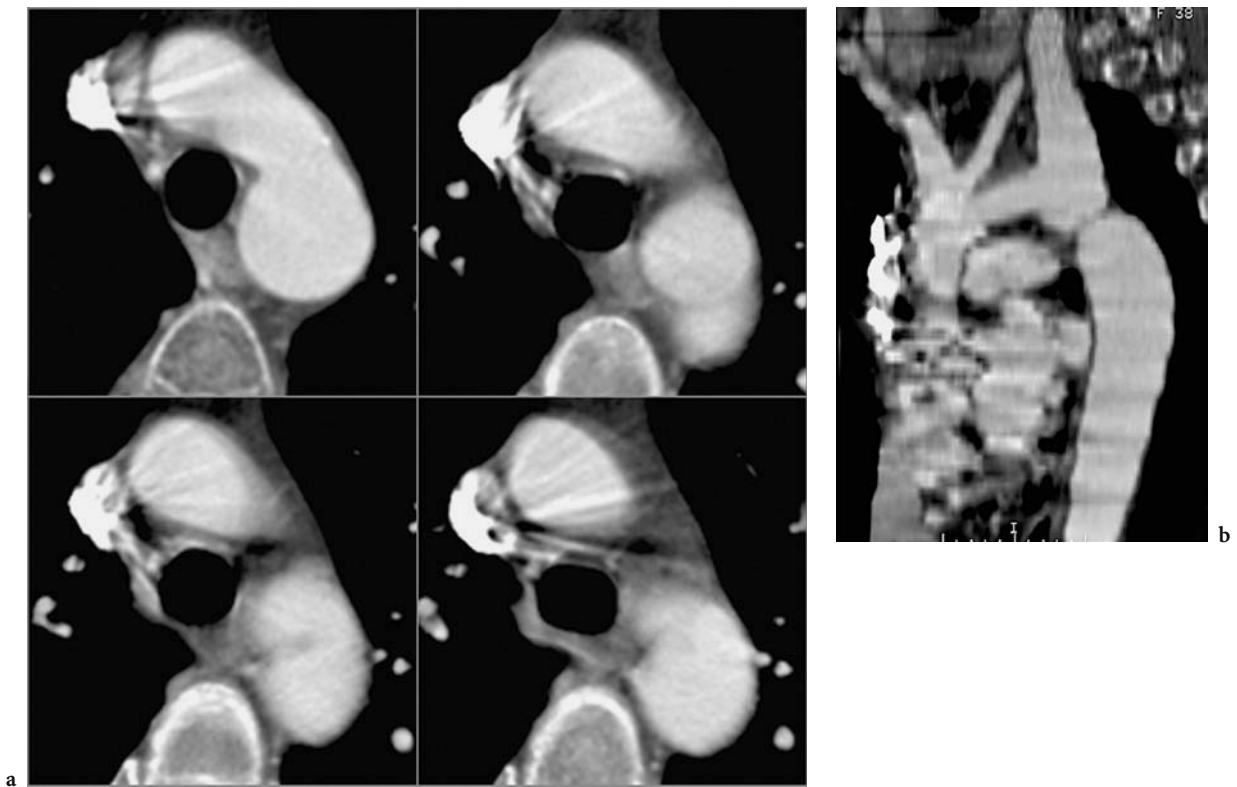
Fig. 20.10. a Consecutive transverse sections acquired with 3 mm collimation, 2.0 pitch demonstrate a linear filling defect in the proximal descending aorta. The lesion is difficult to characterize from the transverse sections alone. **b** Curved planar reformation demonstrates a very short region of aortic coarctation, and a hypoplastic aortic arch with bovine branching pattern and enlarged left subclavian artery

for tracheobronchial narrowing and the presence of aberrant airways. While aortic stenosis secondary to coarctation is clearly demonstrated and enlarged intercostal arteries can be visualized as well, further study must be performed to determine the extent with which the thin webs that often are present in these lesions can be identified and the degree of aortic stenosis determined.

20.8.6
Assessment of Open and Endovascular Interventions

Vascular clips, sternal wires, and graft materials typically result in relatively little artifact on helical CT scans (Fig. 20.11). As a result, helical CTA is an excellent means for assessing the thoracic aorta for perianastomotic complications following aortic or coronary artery bypass graft placement (Fig. 20.12) and complications relating to placement of access cannulas for cardiopulmonary bypass. In fact, the patency of coronary artery bypass grafts often can be determined on helical CT scans and should be routinely examined, particularly in the setting of acute chest pain and the exclusion of aortic dissection as the indication for thoracic CTA.

The CTA is also very useful for the assessment of endoluminal stent grafts (ARMERDING et al. 2000). The success of aneurysm treatment by stent-graft deployment is dependent upon ensuring that the aneurysm has been completely excluded. Perigraft flow can be very slow and thus during flush aortography may be undetected (Fig. 20.13). Because helical CTA relies upon generalized arterial opacification from an intravenous injection rather than a local aortic injection, opacification of perigraft channels are frequently detected on postdeployment CT angiograms, when aortography suggested complete exclusion. Furthermore, because the origins of the brachiocephalic branches are typically tortuous in the setting of thoracic aortic aneurysm, it can be challenging to demonstrate the relationship of the stent graft and the brachiocephalic arterial origins arteriographically. Other complications, such
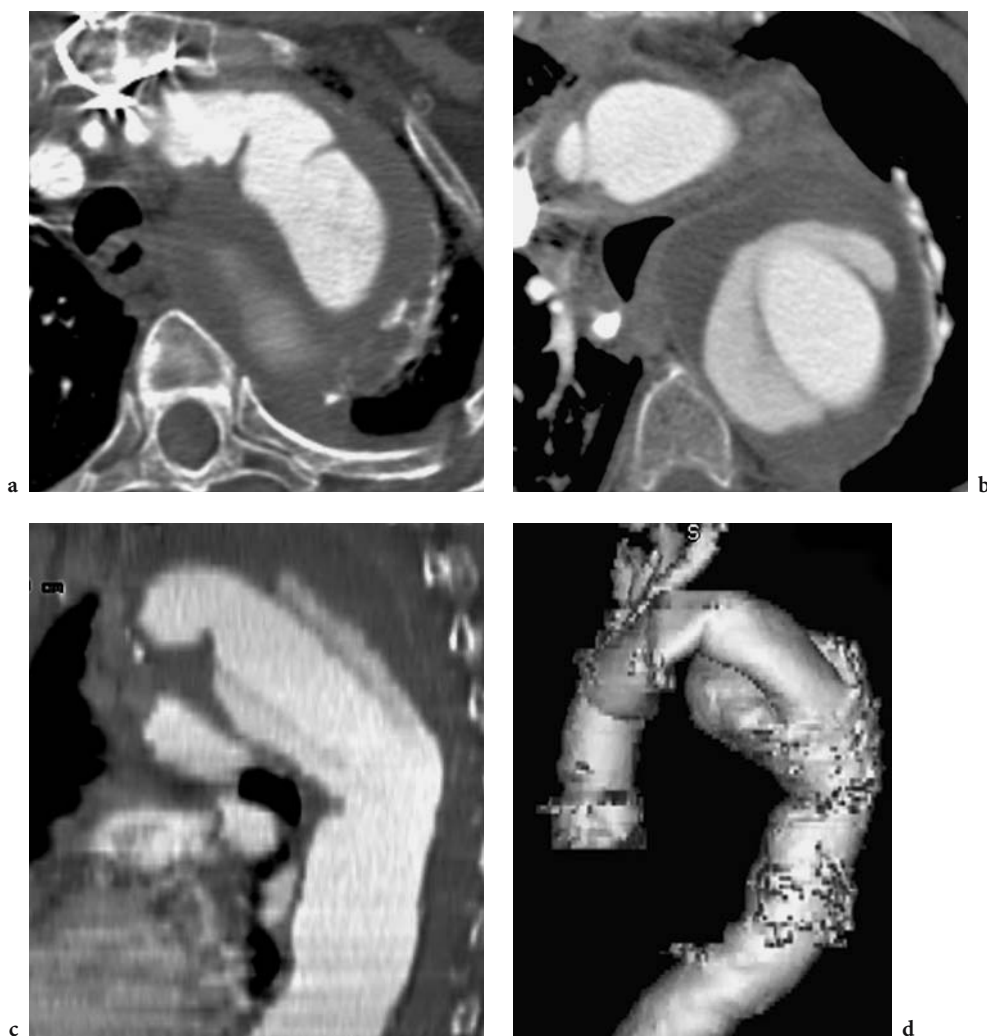
Fig. 20.11. a, b Transverse CT sections to the aortic arch and proximal descending aorta demonstrates the appearance of an elephant-trunk graft which can simulate a primary aortic dissection. Folds in the **a** proximal aspect of the graft mimic intimal flaps, whereas **b** dual-lumen appearance within the descending aorta mimics the true and false lumen of the aortic dissection. **c** Curved planar reformation of the descending aorta demonstrates the characteristic appearance of the elephant-trunk graft extending into the descending aorta. The proximal descending aorta is sutured around the mid graft and a substantial tail of the graft is left within the aortic lumen for subsequent recovery at thoracotomy and placement of an extended descending thoracic aortic graft. **d** Shaded-surface displays facilitate visualization of the complex relationships present in the aortic distal arch. An interposition graft is additionally present in the proximal ascending aorta

as aortic branch occlusions (Fig. 20.14), retroperitoneal hematoma, and iliac arterial dissection or occlusion, are also demonstrable (Fig. 20.15).

20.9
Conclusion

Nine years after its introduction (Napel et al. 1992; Rubin et al. 1993), spiral or helical CTA is being embraced as an important noninvasive tool for imaging the thoracic aorta and its branches. The high degree of accessibility and ease with which the studies are performed make it a viable alternative to aortography. Once familiar with the principles of CTA, the acquisition phase of the examination can be completed in as little as 15 min.

Nevertheless, important challenges remain for CTA. The capabilities of MDCT to acquire thinner sections in shorter scan times have resulted in a veritable explosion of imaging data for radiologists to analyze. In this environment, efficient image processing workstations and software is critical to improving

Fig. 20.12. a Transverse CT sections obtained with 2.5-mm thickness and displayed at 10-mm increments demonstrate a dehisced coronary artery implantation button. The rings of the button are visualized as punctate high-attenuation structures in the *upper left image* (*small arrows*). A 1.5-cm pseudo-aneurysm had formed at the implantation site (*large arrow*). **b–d** Despite the presence of the anastomotic dehiscence in associated pseudo-aneurysm, patency within the right coronary artery is demonstrated (*arrows*)
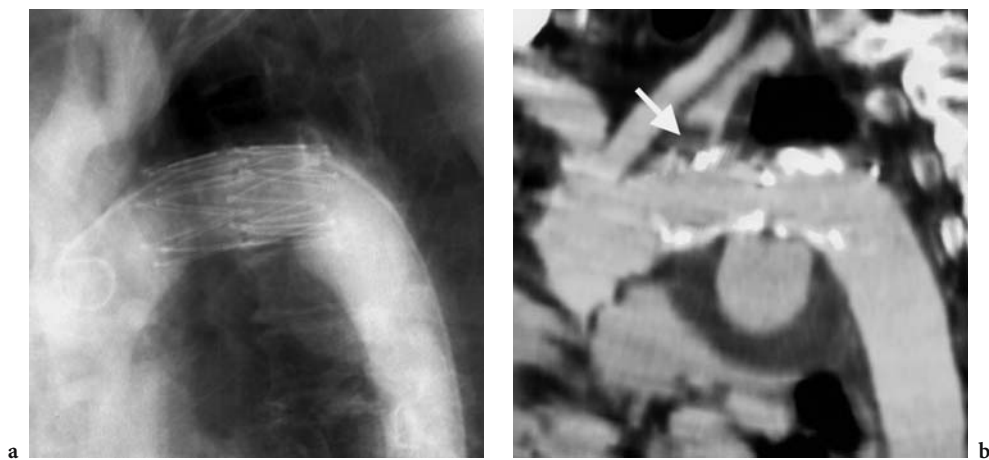

Fig. 20.13. a Aortogram status after deployment of a stent-graft (Dacron covered modified Z stent) over a pseudoaneurysm of at the aortic isthmus. The pseudoaneurysm appears to be completely thrombosed. **b** CPR CTA obtained 4 h after stent-graft deployment demonstrates that the pseudoaneurysm is still patent. Additionally, the stent graft covers the origin of the left subclavian artery, and a thrombus (*arrow*) has formed in the proximal left subclavian artery. The patient underwent transection of the left subclavian artery approximately 5 cm from its origin through a limited incision in the neck. The distal left subclavian artery was transplanted onto the left common carotid artery

our ability to efficiently interpret these volumetric CT data (Rubin et al. 1996a).

Finally, helical CT technology is far from static. Every year new advances in engineering bring better image quality, improved resolution, and faster scan times. As medical imagers, we must not become complacent, but rather constantly challenge ourselves to consider how we might further improve upon our utilization of CT equipment to maximize the collection of information relevant to diagnosis and therapy.
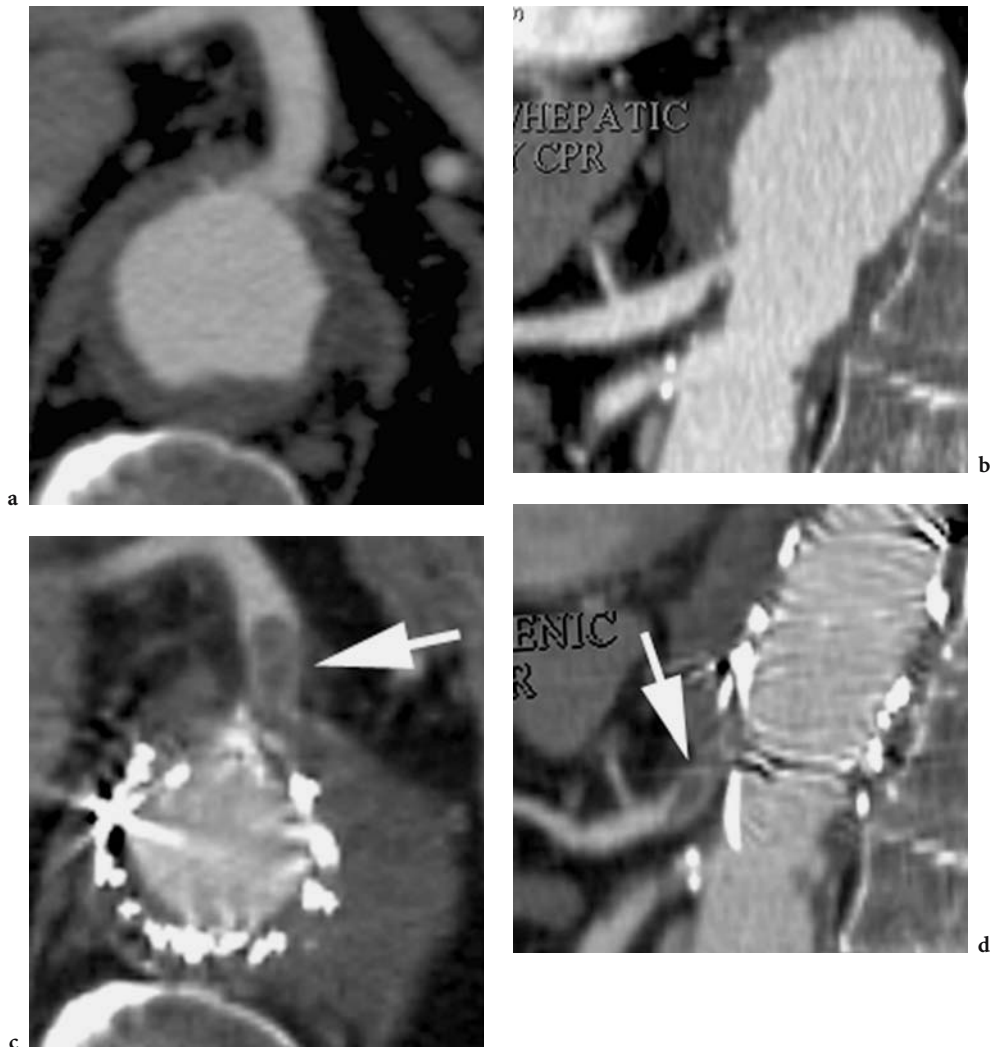

Fig. 20.14. a Transverse sections and **b** curved sagittal reformation through the celiac origin demonstrates a celiac origin stenosis at the distal extent of a thoracoabdominal aortic aneurysm. **c** Transverse CT section and **d** curved sagittal reformation following treatment of the thoracoabdominal aortic aneurysm with a stent graft demonstrates inadvertent occlusion of the celiac origin with thrombus (*arrows*) present in the proximal centimeter of the celiac axis
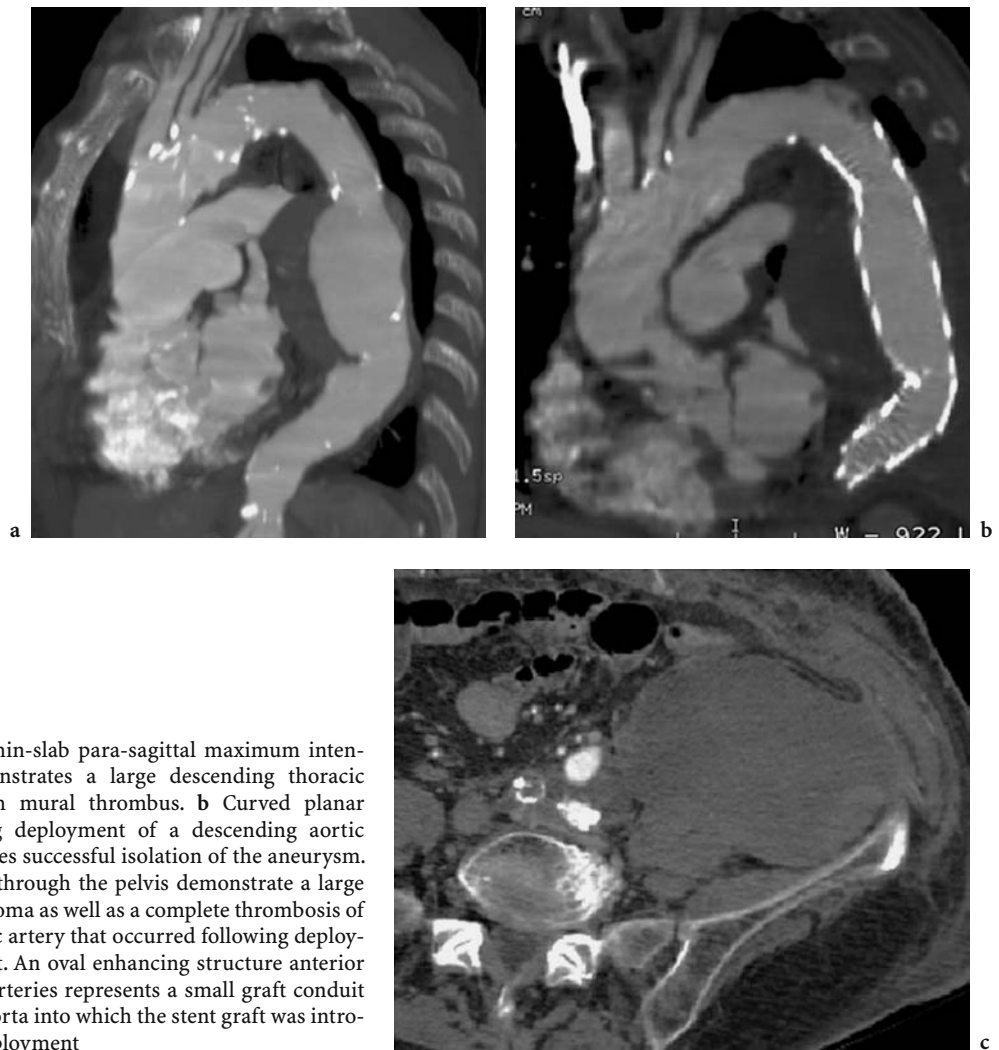
a

b

c

Fig. 20.15. a Curved thin-slab para-sagittal maximum intensity projection demonstrates a large descending thoracic aortic aneurysm with mural thrombus. **b** Curved planar reformation following deployment of a descending aortic stent graft demonstrates successful isolation of the aneurysm. **c** Transverse sections through the pelvis demonstrate a large retroperitoneal hematoma as well as a complete thrombosis of the right common iliac artery that occurred following deployment of the stent graft. An oval enhancing structure anterior to the common iliac arteries represents a small graft conduit sutured to the distal aorta into which the stent graft was introduced for primary deployment

References

Armerding MD, Rubin GD, Beaulieu CF et al. (2000) Aortic aneurysmal disease: assessment of stent-graft treatment-CT versus conventional angiography. Radiology 215: 138–146

Cigarroa JE, Isselbacher EM, DeSanctis RW, Eagle KA (1993) Medical progress. Diagnostic imaging in the evaluation of suspected aortic dissection: old standards and new directions. AJR 161:485–493

Cline HE, Lorensen WE, Souza SP et al. (1991) 3D Surface rendered MR images of the brain and its vasculature. J Comput Assist Tomogr 15:344–351

Dapunt L, Galla JD, Sadeghi AM et al. (1994) The natural history of thoracic aortic aneurysms. J Thorac Cardiovasc Surg 107:1323–1333

Drebin RA, Carpenter L, Hanrahan P (1988) Volume rendering. Comput Graph 22:65–74

Dyer DS, Moore EE, Mestek MF et al. (1999) Can chest CT be used to exclude aortic injury? Radiology 213:195–202

Erbel R, Daniel W, Visser C, Engberding R, Roelandt J, Rennollet H (1989) Echocardiography in diagnosis of aortic dissection. Lancet 4:457–461

Fishman EK, Drebin B, Magid D et al. (1987) Volumetric rendering techniques: applications for three-dimensional imaging of the hip. Radiology 163:737–738

Gavant ML, Manke PG, Fabian T, Flick PA, Graney MJ, Gold RE (1995) Blunt traumatic aortic rupture: detection with helical CT of the chest. Radiology 197:125–133

Gavant ML, Flick P, Manke P, Gold RE (1996) CT aortography of thoracic aortic rupture. AJR 166:955–961

Gore I (1952) Pathogenesis of dissecting aneurysm of the aorta. Arch Pathol Lab Med 53:142–153

Hopkins KL, Patrick LE, Simoneaux SF, Bank ER, Parks WJ, Smith SS (1996) Pediatric great vessel anomalies: initial clinical experience with spiral CT angiography. Radiology 200:811–815

Johnson PT, Heath DG, Bliss DF, Cabral B, Fishman EK (1996) Three-dimensional CT: real-time interactive volume rendering. Am J Roentgenol 167:581–583

Katz M, Konen E, Rozsenman J, Szeinberg A, Itzchak Y (1995) Spiral CT and 3D image reconstruction of vascular ring and associated tracheobronchial anomalies. J Comput Assist Tomogr 19:564–568

Kazerooni EA, Bree RL, Williams DM (1992) Penetrating atherosclerotic ulcers of the descending thoracic aorta: evaluation with CT and distinction from aortic dissection. Radiology 183:759–765

Keller PJ, Drayer BP, Fram EK, Williams KD, Dumoulin CL, Souza SP (1989) MR angiography with two-dimensional acquisition and three-dimensional display. Radiology 173: 527–532

Krinsky GA, Rofsky NM, DeCorato DR et al. (1997) Thoracic aorta: comparison of gadolinium-enhanced three-dimensional MR angiography with conventional MR imaging. Radiology 202:183–193

Kuszyk BS, Heath DG, Bliss DF, Fishman EK (1996) Skeletal 3-D CT: advantages of volume rendering over surface rendering. Skeletal Radiol 25:207–214

Levoy M (1991) Methods for improving the efficiency and versatility of volume rendering. Prog Clin Biol Res 363: 473–488

Magnusson M, Lenz R, Danielsson PE (1991) Evaluation of methods for shaded surface display of CT volumes. Comput Med Imaging Graph 15:247–256

Masuda Y, Takanashi K, Takasu J, Morooka Y, Inagaki Y (1992) Expansion rate of thoracic aortic aneurysms and influencing factors. Chest 102:461–466

Mirvis SE, Shanmuganathan K, Miller BH, White CS, Turney SZ (1996) Traumatic aortic injury: diagnosis with contrast-enhanced thoracic CT: five year experience at a major trauma center. Radiology 200:413–422

Napel S, Marks MP, Rubin GD et al. (1992) CT angiography with spiral CT and maximum intensity projection. Radiology 185:607–610

Napel S, Rubin GD, Jeffrey RB Jr (1993) STS-MIP: a new reconstruction technique for CT of the chest. J Comput Assist Tomogr 17:832–838

Nienaber CA, Kodolitsch Y, Nicolas V et al. (1993) The diagnosis of thoracic aortic dissection by noninvasive imaging procedures. N Engl J Med 328:1–9

Nienaber CA, Kodolitsch Y von, Petersen B et al. (1995) Intramural hemorrhage of the thoracic aorta: diagnostic and therapeutic implications. Circulation 92:1465–1472

Parker MS, Matheson TL, Rao AV et al. (2001) Making the transition: the role of helical CT in the evaluation of potentially acute thoracic aortic injuries. Am J Roentgenol 176:1267–1272

Posniak HV, Olson MC, Demos TC (1993) Aortic motion artifact simulating dissection on CT scans: elimination with reconstructive segmented images. AJR 161:557–558

Prince MR, Narasimham DL, Jacoby WT et al. (1996) Three-dimensional gadolinium-enhanced MR angiography of the thoracic aorta. AJR 166:1387–1397

Prokop M, Schaefer CM, Leppert AGA, Galanski M (1993) Spiral CT angiography of thoracic aorta: femoral or antecubital injection site for intravenous administration of contrast material? Radiology 189:111

Quint LE, Francis IR, Williams DM et al. (1996) Evaluation of thoracic aortic disease with the use of helical CT and multiplanar reconstructions: comparison with surgical findings. Radiology 201:37–41

Raptopoulos V (1994) Chest CT for aortic injury: maybe not for everyone. AJR 162:1053–1055

Remy-Jardin M, Remy J, Wattinne L, Giraud F (1992) Central pulmonary thromboembolism: diagnosis with spiral volumetric CT with the single-breath-hold technique – comparison with pulmonary angiography. Radiology 185:381–387

Rubin GD, Dake MD, Napel SA, McDonnell CH, Jeffrey RBJ (1993) Abdominal spiral CT angiography: initial clinical experience. Radiology 186:147–152

Rubin GD, Dake MD, Napel S et al. (1994) Spiral CT of renal artery stenosis: comparison of three-dimensional rendering techniques. Radiology 190:181–189

Rubin GD, Dake MD, Semba CB (1995) Current status of three-dimensional spiral CT scanning for imaging the vasculature. Radiol Clin North Am 33:51–70

Rubin GD, Lane MJ, Bloch DA, Leung AN, Stark P (1996a) Optimization of contrast enhanced thoracic spiral CT. Radiology 201:785–791

Rubin GD, Beaulieu CF, Argiro V et al. (1996b) Perspective volume rendering of CT and MR images: applications for endoscopic imaging. Radiology 199:321–330

Rubin GD, Shiau MC, Leung AN, Kee ST, Logan LJ, Sofilos MC (2000) Aorta and iliac arteries: single versus multiple detector-row helical CT angiography. Radiology 215:670–676

Rusinek H, Mourino MR, Firooznia H, Weinreb JC, Chase NE (1989) Volumetric rendering of MR images. Radiology 171: 269–272

MDCT of the Heart